Research Square

Preprints are preliminary reports that have not undergone peer review.
They should not be considered conclusive, used to inform clinical practice,
or referenced by the media as validated information.

Systemic inflammatory load index and mortality among US adults: a prospective cohort study of 16,479 NHANES participants(1999- 2010 and 2015-2018)

Jiangbiao Yu
Changde Hospital, Central South University (The first people's hospital of Changde city)
Qingling Peng
Xiangya Hospital Central South University
Yuanyuan Kuang
kuangyy@csu.edu.cn

Xiangya Hospital Central South University

Article

Keywords: systemic inflammation, C-reactive protein, ferritin, neutrophil-to-lymphocyte ratio, all-cause mortality, cardiovascular mortality

Posted Date: November 23rd, 2026

DOI: https://doi.org/10.21203/rs.3.rs-11624054/v1

License: This work is licensed under a Creative Commons Attribution 4.0 International License.
Read Full License

Additional Declarations: No competing interests reported.

Systemic inflammatory load index and mortality among US adults: a prospective cohort study of 16,479 NHANES participants(1999-2010 and 2015-2018)

Jiangbiao Yu[1], Qingling Peng[2], Yuanyuan Kuang[2*]

[1] Department of Cardiology, Changde Hospital, Xiangya School of Medicine, Central South University (The first people's hospital of Changde city), Changde,Hunan, China

[2] Department of Cardiovascular Medicine, Xiangya Hospital, Central South University, Changsha, Hunan, China

*Correspondence: Yuanyuan Kuang E-mail: kuangyy@csu.edu.cn

Abstract

Chronic low-grade inflammation predicts mortality, but each circulating marker reflects only one inflammatory pathway. We built the Systemic Inflammatory Load Index (SILI) from the hepatic acute-phase response (hs-CRP), iron metabolism (ferritin), and innate-adaptive immune activation (NLR), and tested its association with mortality. In 16,479 adults from eight NHANES cycles (2,243 deaths; median follow-up 12.1 years), SILI was the mean of sex-stratified z-scores of the ln-transformed markers. In survey-weighted Cox models, fully adjusted hazard ratios per 1-SD were 1.13 (95% CI 1.06-1.21) for all-cause and 1.13 (1.03-1.25) for cardiovascular mortality; cancer mortality showed no association. The association was nonlinear, rising mainly above roughly 1.6 SD above the cohort median. SILI stayed significant after adjustment for SII, SIRI, or AISI ($P \leq 0.036$), so its signal was not simply the differential count. SILI may be useful as a multi-axis exposure measure, subject to external validation.

Keywords: systemic inflammation, C-reactive protein, ferritin, neutrophil-to-lymphocyte ratio, all-cause mortality, cardiovascular mortality

Abbreviations

- SILI, Systemic Inflammatory Load Index; hs-CRP, high-sensitivity C-reactive protein; NLR, neutrophil-to-lymphocyte ratio; NHANES, National Health and Nutrition Examination Survey; NDI, National Death Index; MEC, Mobile Examination Center; HR, hazard ratio; CI, confidence interval; CVD, cardiovascular disease; BMI, body mass index; MI, multiple imputation; RCS, restricted cubic spline; PIR, poverty-income ratio; SII, systemic immune-inflammation index; SIRI, systemic inflammation response index; AISI, aggregate index of systemic inflammation; NRI, net reclassification improvement; IDI, integrated discrimination improvement; RMST, restricted mean survival time; AUC, area under the receiver-operating-characteristic curve; DCA, decision-curve analysis; IPCW, inverse probability of censoring

weights; SHR, subdistribution hazard ratio; FDR, false discovery rate; HbA1c, glycated hemoglobin; HDL, high-density lipoprotein cholesterol; CDC, Centers for Disease Control and Prevention; AHA, American Heart Association; NCHS, National Center for Health Statistics; SE, standard error; C-index, Harrell concordance index; ΔC, change in C-index; LRT, likelihood-ratio test; RERI, relative excess risk due to interaction; SBP, systolic blood pressure; DBP, diastolic blood pressure.

Introduction

Chronic low-grade inflammation is now widely seen as a shared biological thread in ageing and in chronic disease, including atherosclerosis, type 2 diabetes, cancer, and frailty [1,2]. For three decades, epidemiological work has looked for circulating markers that capture this burden and predict outcomes [3]. One candidate, high-sensitivity C-reactive protein (hs-CRP), is a classical hepatic acute-phase reactant and independently predicts cardiovascular events and death [4,5]. The neutrophil-to-lymphocyte ratio (NLR), drawn from the routine differential count, has become a widely used prognostic marker in cardiovascular disease and cancer [6,7]. Serum ferritin, an acute-phase protein that also reflects iron stores, has been linked to atherosclerosis and cardiometabolic risk in several population studies [8-10].

These single-marker approaches have a clear weakness: systemic inflammation is not one pathway. hs-CRP tracks hepatocyte output driven largely by interleukin-6. Ferritin reflects iron stores plus the reticuloendothelial acute-phase response, while NLR arises from bone-marrow myelopoiesis and lymphocyte dynamics under chronic antigenic and stress stimulation [11-13]. Because these compartments answer to partly different upstream signals, a single marker can misclassify people whose inflammatory burden is spread across pathways. Composite indices that combine axes do show prognostic value, but the ones proposed so far draw only on the differential blood count and so capture just the cellular arm of inflammation: the systemic immune-inflammation index (SII,

platelet×neutrophil/lymphocyte) [14], the systemic inflammation response index (SIRI, neutrophil×monocyte/lymphocyte) [15], and the aggregate index of systemic inflammation (AISI, platelet×neutrophil×monocyte/lymphocyte) [16]. Being built entirely from blood-count data, SII and SIRI carry no information about the hepatic acute-phase response or iron-metabolic inflammation, two axes with well-established links to mortality. No index spanning the hepatic, iron-metabolic, and cellular arms has yet been tested against hard mortality endpoints in a nationally representative sample, and existing composites have rarely been compared head-to-head within one cohort, where differing study populations and covariate sets make their hazard ratios hard to line up.

We therefore built a simple composite, the Systemic Inflammatory Load Index (SILI), as the mean of sex-stratified z-scores of ln-transformed hs-CRP, ferritin, and NLR, and tested it against all-cause, cardiovascular, and cancer mortality in a pooled, mortality-linked sample from eight NHANES cycles with up to two decades of follow-up. To set SILI beside the existing markers, we compared it directly with hs-CRP, ferritin, NLR, SII, SIRI, and AISI in the same sample and fitted mutually adjusted models. We also looked at incremental predictive performance through reclassification, time-dependent discrimination, calibration, and decision-curve metrics, examined the threshold pattern suggested by the spline, expressed the association in absolute terms as a difference in restricted mean survival time, and checked robustness with time-split estimation, a negative-control outcome, alternative standardization, and E-values. SILI is not offered as a replacement for hs-CRP in risk prediction. Its purpose is to be a single exposure measure that summarises three partly independent inflammatory axes for etiological research, so we benchmark it against hs-CRP rather than against a prediction model.

Results

Baseline characteristics

A total of 16,479 adults were included, representing a weighted US population of 95 million. Over a median follow-up of 12.1 years (unweighted; 13.2 years weighted), 2,243 deaths occurred, including 685 cardiovascular and 500 cancer deaths. As shown in Table 1, the general characteristics of participants were summarized according to quartiles of SILI: Q1 (<−0.407), Q2 (−0.407-0.003), Q3 (0.003-0.400), and Q4 (≥0.400). Specifically, participants in the highest quartile of SILI were more likely to be older (weighted mean age, 48.2 vs 37.8 years in the lowest quartile), have higher BMI (31.3 vs 25.6 kg/m²), higher HbA1c (5.69 vs 5.26%), and higher prevalences of diabetes (14.5% vs 2.9%) and hypertension (35.2% vs 13.9%), and showed a less favorable lipid profile. In contrast, those in the lowest quartile tended to be younger and had lower BMI, HbA1c, and lower prevalences of diabetes and hypertension. Mean component values increased monotonically across quartiles (hs-CRP 0.20 to 2.40 mg/L; ferritin 52 to 184 ng/mL; NLR 1.58 to 2.87). Women constituted 67.2% of the weighted sample (66.4% unweighted), a direct consequence of NHANES ferritin assay eligibility: serum ferritin was measured in all adults in 1999-2002 and 2017-2018 but only in women of childbearing age (12-49 years) in the five intermediate cycles (2003-2004, 2005-2006, 2007-2008, 2009-2010, and 2015-2016), so participants from those five cycles are women aged 20-49 years (Methods, Study design and population). Moreover, the three z-scored components were only weakly correlated with one another (survey-weighted Pearson r=0.17 for hs-CRP vs ferritin, 0.07 for hs-CRP vs NLR, and −0.03 for ferritin vs NLR; similar by sex; Supplementary Table S1), indicating that each carries largely non-redundant information and that collinearity is not a concern for the composite.

Table 1. Weighted baseline characteristics of US adults by quartiles of the Systemic Inflammatory Load Index (SILI), NHANES 1999-2010 and 2015-2018.

Characteristic	Total	Q1[−2.72−0.407]	Q2(−0.407,0.003]	Q3(0.003,0.400]	Q4(0.400,3.14]	P value
	n=16,479	n=4,118	n=4,153	n=4,076	n=4,132	
Age, years	42.5±0.25	37.8±0.26	40.2±0.31	43.7±0.38	48.2±0.44	<0.001
Body mass index, kg/m²	28.3±0.10	25.6±0.12	27.4±0.12	29.1±0.13	31.3±0.21	<0.001
Poverty-income ratio	2.98±0.04	3.01±0.05	2.97±0.05	3.01 ± 0.04	2.93±0.04	0.262
HbA1c, %	5.44±0.01	5.26±0.01	5.35± 0.02	5.48 ± 0.02	5.69±0.02	<0.001
HDL cholesterol, mg/dL	53.9±0.26	56.1±0.45	54.3±0.38	53.5 ± 0.35	51.7±0.33	<0.001
hs-CRP, mg/L	1.03±0.02	0.20±0.01	0.50±0.02	1.02 ± 0.03	2.40±0.06	<0.001
Ferritin, ng/mL	109.5±1.55	52.5±1.12	85.8±1.44	115.3±2.70	184.3±4.69	<0.001
Neutrophil-to-lymphocyte ratio	2.14±0.01	1.58±0.01	1.93±0.01	2.20±0.02	2.87±0.03	<0.001
Sex						0.868
Female	11,069 (67.2)	2,782 (67.6)	2,763 (66.5)	2,735 (67.1)	2,790 (67.5)	
Male	5,410 (32.8)	1,336 (32.4)	1,390 (33.5)	1,341 (32.9)	1,342 (32.5)	
Race/ethnicity						<0.001
Non-Hispanic White	11,267 (68.4)	2,655 (64.5)	2,814 (67.8)	2,866 (70.3)	2,930 (70.9)	
Non-Hispanic Black	1,777 (10.8)	608 (14.8)	441 (10.6)	379 (9.3)	350 (8.5)	
Mexican American	1,308 (7.9)	325 (7.9)	354 (8.5)	326 (8.0)	303 (7.3)	
Other Hispanic	1,035 (6.3)	275 (6.7)	263 (6.3)	237 (5.8)	260 (6.3)	
Other	1,092 (6.6)	255 (6.2)	281 (6.8)	268 (6.6)	289 (7.0)	
Education						<0.001
<9th grade	801 (4.9)	199 (4.8)	215 (5.2)	194 (4.8)	193 (4.7)	
9-12th grade	1,827 (11.1)	454 (11.0)	457 (11.0)	461 (11.3)	454 (11.0)	
High school	3,986 (24.2)	832 (20.2)	972 (23.4)	1,022 (25.1)	1,160 (28.1)	
Some college	5,208 (31.6)	1,302 (31.6)	1,318 (31.7)	1,229 (30.1)	1,361 (32.9)	
≥College	4,657 (28.3)	1,331 (32.3)	1,191 (28.7)	1,170 (28.7)	964 (23.3)	
Smoking status						<0.001
Never	9,164 (55.6)	2,465 (59.9)	2,328 (56.1)	2,217 (54.4)	2,153 (52.1)	
Former	3,540 (21.5)	810 (19.7)	853 (20.5)	824 (20.2)	1,055 (25.5)	
Current	3,775 (22.9)	843 (20.5)	972 (23.4)	1,035 (25.4)	924 (22.4)	
Diabetes						<0.001
Yes	1,259 (7.6)	121 (2.9)	222 (5.3)	316 (7.8)	600 (14.5)	
No	15,220 (92.4)	3,997 (97.1)	3,931 (94.7)	3,760 (92.2)	3,532 (85.5)	
Hypertension						<0.001
Yes	3,775 (22.9)	571 (13.9)	762 (18.3)	987 (24.2)	1,454 (35.2)	
No	12,704 (77.1)	3,547 (86.1)	3,391 (81.7)	3,089 (75.8)	2,678 (64.8)	

Data are presented as weighted mean ± standard error (SE) for continuous variables or as n (%) for categorical variables; the n are unweighted numbers of participants and the percentages are survey-weighted, so percentages are computed on the weighted distribution and do not necessarily sum to exactly 100 within a row after rounding. Quartile cut-points of SILI: −0.407, 0.003, 0.400. Weighted population 95 million; n=16,479. The sample is 67.2% women because the NHANES ferritin assay was restricted to women of childbearing age (12-49 years) in the five intermediate cycles (2003-2004, 2005-2006, 2007-2008, 2009-2010, and 2015-2016); see Methods, Study design and population. Differences in continuous variables were assessed using one-way ANOVA for normally distributed variables and the Kruskal-Wallis test for non-normally distributed variables.

SILI and mortality

Over a median follow-up of 12.1 years, a total of 2,243 deaths occurred, including 685 cardiovascular and 500 cancer deaths. Survey-weighted Cox regression analysis demonstrated that SILI was positively associated with all-cause mortality. In the crude model, the association was strongest (per-SD HR=1.62, 95% CI: 1.52-1.72; P<0.001), and it attenuated progressively across Models 1 and 2, a pattern consistent with confounding, principally by age and cardiometabolic factors. In the age-, sex-, and race/ethnicity-adjusted model, each 1-SD increment was associated with a 24% higher risk (HR=1.24, 95% CI: 1.15-1.33; P<0.001). After full adjustment for socioeconomic, anthropometric, and cardiometabolic factors, the association was attenuated but remained significant (HR=1.13, 95% CI: 1.06-1.21; P=0.0002), and further adjustment for baseline prevalent cardiovascular disease and cancer (Model 3) did not materially change the estimate (HR=1.14, 95% CI: 1.07-1.22). In total, approximately 75% of the crude log-hazard-ratio was attenuated across the adjustment sequence. The association was graded across quartiles: compared with the lowest quartile, HRs were 1.02 (95% CI: 0.87-1.19), 1.10 (95% CI: 0.94-1.29), and 1.23 (95% CI: 1.06-1.44) in increasing quartiles (P for trend=0.004; Table 2). Kaplan-Meier curves showed progressively lower cumulative survival with higher SILI quartile for both all-cause and cardiovascular mortality (Figure 2). Expressed in absolute terms, the fully adjusted restricted mean survival time over 12 years was 2.31 months shorter in the highest than in the

lowest SILI quartile (95% CI: 1.25-3.37 months; P<0.001). A separate parametrization with continuous SILI entered linearly instead of as quartile indicators yielded a loss of 1.01 months per 1-SD increment (95% CI: 0.66-1.36; P<0.001). These two absolute measures are not linearly convertible because the dose-response is threshold-shaped, with risk negligible across most of the distribution and concentrated at its upper end.

For cardiovascular mortality, the fully adjusted HR per SD was 1.13 (95% CI: 1.03-1.25; P=0.011), with Q4 vs Q1 HR=1.33 (95% CI: 1.00-1.77; P=0.050) and P for trend=0.045; Model 3 estimates were similar (per SD, 1.15; 95% CI: 1.04-1.27). In contrast, SILI was not associated with cancer mortality (per-SD HR=1.03, 95% CI: 0.88-1.21; P=0.72; Table 2).

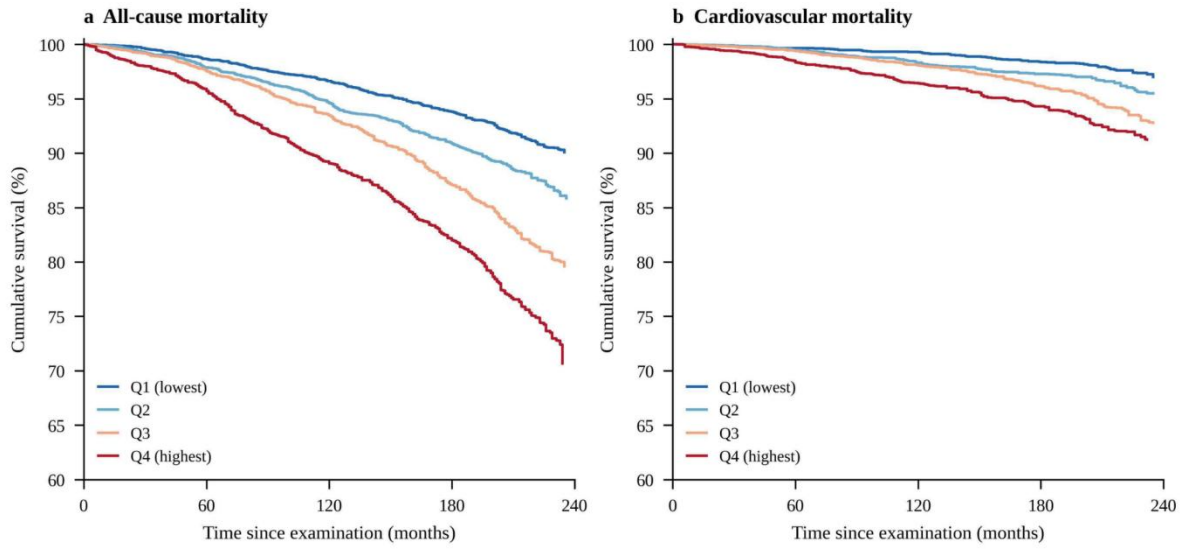


Figure 2. Inverse-probability-weighted Kaplan-Meier estimates of cumulative survival by SILI quartile for all-cause (a) and cardiovascular (b) mortality. Curves truncated at 236 months.

Table 2. Association between the Systemic Inflammatory Load Index (SILI) and mortality, NHANES 1999-2010 and 2015-2018.

	Crude model		Model 1		Model 2		Model 3	
	HR (95% CI)	**P**	**HR (95% CI)**	**P**	**HR (95% CI)**	**P**	**HR (95% CI)**	**P**
All-cause mortality (2,243 deaths)								
Per 1-SD increment	1.62(1.52-1.72)	<0.001	1.24(1.15-1.33)	<0.001	1.13(1.06-1.21)	0.0002	1.14(1.07-1.22)	<0.001
Q1 (reference)	1.00		1.00		1.00		1.00	
Q2	1.46(1.29-1.65)	<0.001	1.12(0.97-1.30)	0.13	1.02(0.87-1.19)	0.81	1.04(0.88-1.22)	0.67
Q3	2.12(1.79-2.51)	<0.001	1.29(1.11-1.51)	0.001	1.10(0.94-1.29)	0.22	1.13(0.97-1.31)	0.12
Q4	3.28(2.84-3.78)	<0.001	1.57(1.33-1.86)	<0.001	1.23(1.06-1.44)	0.008	1.27(1.09-1.48)	0.002
P for trend		<0.001		<0.001		0.004		0.001
Cardiovascular mortality (685 deaths)								
Per 1-SD increment	1.66(1.53-1.80)	<0.001	1.26(1.14-1.39)	<0.001	1.13(1.03-1.25)	0.011	1.15(1.04-1.27)	0.006
Q1 (reference)	1.00		1.00		1.00		1.00	
Q2	1.68(1.23-2.31)	0.001	1.27(0.90-1.80)	0.18	1.16(0.84-1.60)	0.38	1.16(0.86-1.57)	0.32
Q3	2.49(1.75-3.55)	<0.001	1.47(1.04-2.08)	0.030	1.24(0.90-1.71)	0.19	1.28(0.93-1.77)	0.13
Q4	3.78(2.87-4.96)	<0.001	1.76(1.30-2.37)	<0.001	1.33(1.00-1.77)	0.050	1.40(1.06-1.85)	0.017
P for trend		<0.001		<0.001		0.045		0.016
Cancer mortality (500 deaths)								
Per 1-SD increment	1.39(1.21-1.60)	<0.001	1.11(0.94-1.30)	0.22	1.03(0.88-1.21)	0.72	1.04(0.88-1.22)	0.66
Q1 (reference)	1.00		1.00		1.00		1.00	
Q2	1.23(0.88-1.70)	0.22	0.99(0.69-1.42)	0.95	0.91(0.64-1.30)	0.60	0.93(0.65-1.33)	0.68
Q3	1.77(1.32-2.38)	<0.001	1.17(0.86-1.59)	0.32	1.00(0.73-1.36)	0.99	1.02(0.75-1.38)	0.91
Q4	2.13(1.57-2.90)	<0.001	1.15(0.82-1.62)	0.42	0.94(0.68-1.32)	0.74	0.97(0.69-1.35)	0.84
P for trend		<0.001		0.24		0.91		0.99

Crude model: unadjusted.

Model 1: adjusted for age, sex, race/ethnicity.

Model 2: additionally adjusted for education, poverty-income ratio, BMI, smoking, diabetes, hypertension (primary fully adjusted model).

Model 3: additionally adjusted for baseline prevalent cardiovascular disease and cancer.

Survey-weighted Cox models; per SD=per 1-SD increment of SILI (SD=0.61); quartile cut-points of SILI: −0.407, 0.003, 0.400;

P for trend=test for linear trend with SILI quartiles entered as an ordinal integer variable.

CI, confidence interval.

Cancer mortality was based on n=500 deaths; with only 500 events this secondary outcome has limited statistical power, and its null estimates should be read as neither demonstrating an association nor excluding a moderate one.

Non-linear dose-response

As shown in Figure 3, RCS analyses showed that the relationships between SILI and all-cause and cardiovascular mortality were nonlinear (P for non-linearity<0.001 and P=0.047, respectively). Specifically, the relationship was J-shaped, with HRs flat and slightly below 1 across the lower half of the SILI distribution and risk increasing above approximately 0.5-0.8 SD above the cohort median. The sub-unity HRs in the low-SILI region should not be interpreted as evidence of protection; this pattern likely reflects regression dilution from single baseline measurements, and the only defensible reading is that no excess mortality risk was detectable in that range.

A two-piecewise Cox model formalized this pattern (Supplementary Table S2). With a single sharp change point, the best-supported breakpoint fell above the visual inflection zone: SILI=0.98, roughly 1.6 SD above the cohort median. Improvement over a single-line model was highly significant (design-based likelihood-ratio test, P<0.001). The two approaches are consistent: the flexible spline picks up the onset of risk earlier (0.5-0.8 SD above the median), while the two-piecewise model places the threshold at the point of maximal slope change (1.6 SD). Either way, risk is negligible across most of the distribution and concentrated at the upper end. Below the breakpoint, the hazard ratio per 1-unit increment (one unit≈ 1.64 SD) was flat and nonsignificant (1.09; 95% CI, 0.98-1.21); above it, each additional unit was associated with a 6.3-fold hazard (6.27; 4.05-9.72). Cardiovascular mortality selected the same breakpoint, with a flat lower segment (1.08; 0.92-1.27) and a steep upper segment (7.01; 3.28-14.98; P=0.001). In this cohort, the dose-response relationship is better described as a threshold than as a graded linear effect, with excess risk concentrated in individuals whose inflammatory load exceeds about 1.6 SD above the median. Above the breakpoint there were 821 participants (weighted population 4.6 million; 4.8% of the cohort) with 158 deaths (55 cardiovascular, 33 cancer), a crude death proportion of 19.2% versus 13.3% below

the breakpoint. Because the breakpoint was selected data-driven, we repeated the two-piecewise model at two thresholds fixed in advance of any outcome inspection: 1.0 SD above the cohort median (SILI=0.61; 2,502 participants, 426 deaths) and 1.5 SD (SILI=0.91; 1,015 participants, 188 deaths). Both reproduced the pattern, with upper-segment hazard ratios of 2.53 (1.75-3.65; P<0.001) and 5.15 (3.33-7.95; P<0.001) and highly significant improvement over a single-line model (P=1.0 x 10^{-5} and 4.4 x 10^{-8}, respectively).

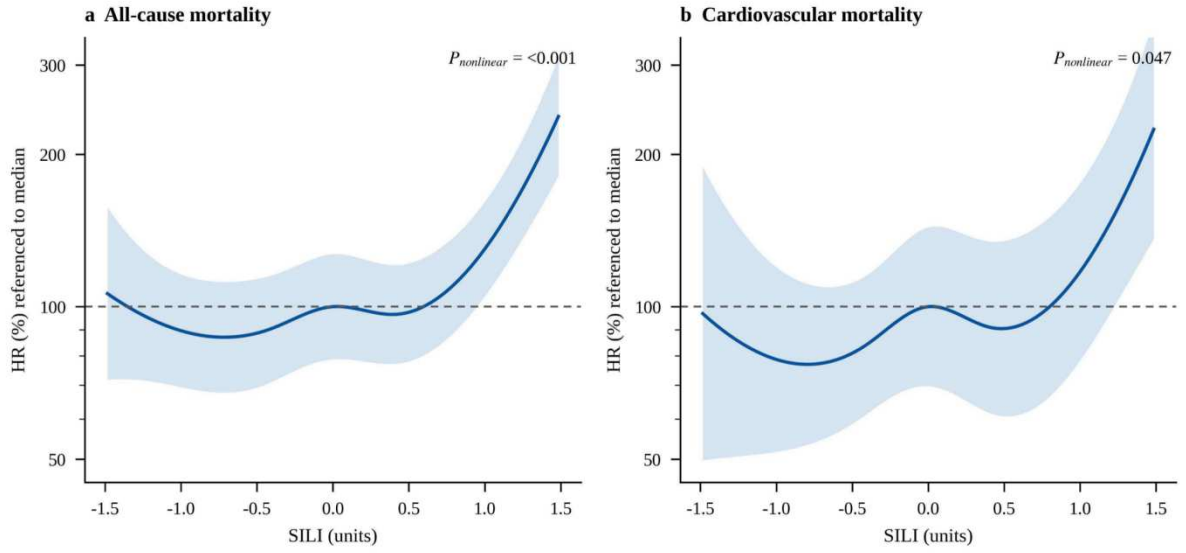


Figure 3. Restricted cubic spline analysis of the association between SILI and all-cause (a) and cardiovascular (b) mortality. Hazard ratios (solid line) and 95% confidence bands (shaded area) are referenced to the cohort median SILI; fitted with a natural spline (equivalently, a restricted cubic spline, RCS) with internal knots at the 25th, 50th, and 75th percentiles and boundary knots at the observed minimum and maximum; the y-axis is on a logarithmic scale; the x-axis is truncated to ±1.5 SILI units (≈±2.5 SD of SILI; the between-person SD of SILI is 0.61) to avoid unstable extrapolation at the distribution tails. The sub-unity hazard ratios in the low-SILI region reflect regression dilution from a single baseline measurement and should not be read as evidence of protection.

Subgroup analyses

In subgroup analyses, the association was directionally consistent across all prespecified subgroups (Supplementary Figure S5). Among the eight interaction tests, only age showed a significant interaction after Benjamini-Hochberg correction (crude P=0.006, corrected q=0.045), with a stronger association in participants<60 years (HR, 1.22; 1.10-1.35) than ≥60

years (HR, 1.18; 1.10-1.28). The absolute difference between the two hazard ratios is small and their confidence intervals overlap substantially; although the interaction withstood FDR correction, we regard it as a preliminary, hypothesis-generating finding that must be replicated in external cohorts before any biological interpretation is attached to it. All other interactions were clearly null (corrected q≥0.84); the full set of interaction tests before and after FDR correction is displayed in Supplementary Figure S4.

Sensitivity analyses and single components

The primary association held in most prespecified sensitivity analyses (Supplementary Table S4). Two estimates were imprecise rather than inconsistent: the 2015-2018 era estimate (HR, 1.26; 0.87-1.81; only 82 deaths) did not reach statistical significance, and the Fine-Gray subdistribution HR for cardiovascular mortality (1.08; 0.99-1.16; P= 0.071) was directionally consistent but not significant. The accidental-death negative control was null by design (P=0.54). Censoring at 24 months (HR, 1.09; 1.02-1.16) and restricting to hs-CRP≤3mg/L (HR, 1.10; 1.04-1.18) did not eliminate the association. Excluding prevalent cardiovascular disease, cancer, or both gave HRs of 1.13 (1.05-1.21), 1.11 (1.03-1.19), and 1.10 (1.02-1.19). Multiple imputation in the pre-MI sample (n=18,635) yielded HR 1.16 (1.10-1.22); m=20 gave nearly identical results. Restricting to the three ferritin-complete cycles (n=11,008; 2,130 deaths) gave HR 1.18 (1.10-1.26). The accidental-death negative control also merits comment: its point estimate was 1.11 (0.80-1.55) rather than exactly 1.0, but with only 85 accidental deaths the interval is wide and fully compatible with no association; the purpose of a negative control is to show that the exposure is not meaningfully associated with an outcome it cannot plausibly cause, which both the interval and the P value support. An estimate modestly above unity is expected for a rare outcome in an exposure correlated with general frailty, and it is far weaker than the main association. Finally, to address residual confounding by imperfectly measured hypertension, additional adjustment for measured

systolic and diastolic blood pressure and current antihypertensive medication left the estimate essentially unchanged (n=15,871; HR 1.13; 95%CI, 1.06-1.21; P<0.001), as did the cardiovascular estimate (1.12; 1.02-1.23; P=0.019).

The Fine-Gray SHR (1.08) was smaller and less precise than the cause-specific HR (1.13; P=0.011), as expected because they answer different questions. Competing deaths deplete the subdistribution risk set in higher-SILI individuals, pulling the SHR toward the null. Survey-weighted Aalen-Johansen functions show this: 10-year cardiovascular death incidence rose across SILI quartiles (0.70%, 1.66%, 1.87%, 3.48%), while non-cardiovascular death remained more common in every quartile (2.68% to 7.53%). Both approaches point in the same direction, but the cardiovascular finding should be considered directional rather than definitive.

Individually, hs-CRP (HR, 1.20; 1.11-1.29) and NLR (1.11; 1.05-1.18) were associated with all-cause mortality; ferritin was not (0.99; 0.93-1.04). Comparisons with SII, SIRI, and AISI appear in the benchmarking analysis below and in Table 3.

The base model C-index was 0.873; adding SILI changed it by +0.00003, and hs-CRP by +0.0009. The high absolute C-index largely reflects age(age alone, C=0.842; model without age, C=0.767, rising to 0.778 with SILI). These increments are clinically negligible(all $|\Delta C| < 0.001$). The near-zero ΔC does not mean SILI lacks biological relevance; it means SILI cannot improve individual-level discrimination beyond conventional risk factors, a distinction formalized in the benchmarking analysis.

Two additional analyses addressed index construction and robustness (Supplementary Table S4). SILI-2, excluding ferritin (r=0.84 with SILI), gave slightly stronger associations (all-cause HR, 1.18; 1.11-1.25; cardiovascular HR, 1.21; 1.10-1.33), indicating modest dilution from equal-weight ferritin. Era-stratified estimates were similar: 1999-2010 HR 1.13 (1.05-

1.21; n=11,645; 2,161 deaths) and 2015-2018 HR 1.26 (0.87-1.81; n =4,834; 82 deaths). The pooled estimate was not driven by either era, though limited precision after 2015 means modest drift cannot be excluded (Discussion, Strengths and limitations).

Benchmarking against alternative markers and robustness

Head-to-head benchmark. In the same analytic sample and with the same Model 2 covariates, SILI had the highest point estimate among the three composites, although hs-CRP remained the strongest single marker (Table 3). Fully adjusted all-cause hazard ratios per 1-SD were 1.13 (1.06-1.21) for SILI, 1.20 (1.11-1.29) for hs-CRP, 0.99 (0.93-1.04) for ferritin, 1.11 (1.05-1.18) for NLR, 1.06 (1.00-1.13) for SII, 1.12 (1.05-1.19) for SIRI, and 1.07 (1.01-1.13) for AISI. For cardiovascular mortality, SILI (1.13; 1.03-1.25) was comparable to hs-CRP (1.16; 1.01-1.34) and NLR (1.17; 1.07-1.27). No marker was associated with cancer mortality. Time-dependent AUC curves for all seven markers are shown in Supplementary Figure S3.

Table 3. Head-to-head benchmark of the Systemic Inflammatory Load Index (SILI) against single inflammatory markers and alternative composite indices (Model 2, per 1-SD increment).

Marker	All-cause mortality		Cardiovascular mortality		Cancer mortality		ΔC-index
	HR (95% CI)	P	HR (95% CI)	P	HR (95% CI)	P	
SILI (hs-CRP + ferritin + NLR)	1.13 (1.06-1.21)	0.0002	1.13 (1.03-1.25)	0.011	1.03 (0.88-1.21)	0.72	+0.00003
hs-CRP (single marker)	1.20 (1.11-1.29)	<0.001	1.16 (1.01-1.34)	0.042	1.12 (0.94-1.32)	0.20	+0.00087
Ferritin (single marker)	0.99 (0.93-1.04)	0.62	0.95 (0.88-1.03)	0.23	0.95 (0.85-1.08)	0.45	+0.00001
NLR (single marker)	1.11 (1.05-1.18)	<0.001	1.17 (1.07-1.27)	<0.001	1.03 (0.90-1.19)	0.65	−0.00040
SII (platelet× neutrophil / lymphocyte)	1.06 (1.00-1.13)	0.052	1.09 (0.99-1.19)	0.072	0.96 (0.85-1.09)	0.55	−0.00028
SIRI (neutrophil× monocyte / lymphocyte)	1.12 (1.05-1.19)	<0.001	1.14 (1.03-1.26)	0.014	1.00 (0.89-1.13)	0.96	−0.00045
AISI (platelet× neutrophil× monocyte / lymphocyte)	1.07 (1.01-1.13)	0.023	1.07 (0.97-1.18)	0.20	0.95 (0.84-1.07)	0.38	−0.00033

All estimates are from survey-weighted Cox models adjusted as in Model 2. Every marker was ln-transformed, standardized within sex against the analytic sample (n=16,479), and entered per 1-SD increment, so that hazard ratios are directly comparable across rows. ΔC-index is the change in Harrell concordance index relative to the base covariate model (C=0.873) on addition of that marker alone, reported to five decimal places because the increments are small by an order of magnitude against a base model that already contains age; the high absolute C-index itself reflects the dominant contribution of age (age alone, C=0.842; covariates without age, C=0.767, rising to 0.778 with SILI).

The mutually adjusted models were the most revealing part of this comparison. When SILI was entered with each differential-count composite in turn, it remained significant in every all-cause model: adjusted for SII, 1.14 (95% CI, 1.04-1.25; P=0.005); for SIRI, 1.09 (1.01-1.18; P=0.036); for AISI, 1.13 (1.04-1.22; P=0.004). The competing index was attenuated to non-significance in each case (SII, 0.99, P=0.89; SIRI, 1.06, P=0.10; AISI, 1.01, P=0.76; Table 4). The contrast was weaker for cardiovascular mortality: SILI remained significant only after adjustment for AISI (1.13; 1.01-1.25; P=0.031), while in the SILI-SII (P=0.10) and SILI-SIRI (P=0.20) models neither index reached significance. Because SII, SIRI, and AISI are algebraic functions of the same differential count and therefore highly correlated, the all-cause results suggest that, once the hepatic and iron-metabolic axes are included, the purely cellular composites add little on their own, but not the reverse. This supports the construct rationale for SILI: adding hs-CRP and ferritin to the cellular axis is not redundant.

Table 4. Mutually adjusted models of the Systemic Inflammatory Load Index (SILI) with each differential-count composite index (Model 2, per 1-SD increment).

Model	All-cause HR (95% CI)	P	CVD HR (95% CI)	P
SILI mutually adjusted for SII	1.14 (1.04-1.25)	0.005	1.11 (0.98-1.25)	0.10
SII mutually adjusted for SILI	0.99 (0.92-1.08)	0.89	1.03 (0.92-1.16)	0.57
SILI mutually adjusted for SIRI	1.09 (1.01-1.18)	0.036	1.07 (0.97-1.19)	0.20
SIRI mutually adjusted for SILI	1.06 (0.99-1.15)	0.10	1.09 (0.98-1.23)	0.12
SILI mutually adjusted for AISI	1.13 (1.04-1.22)	0.004	1.13 (1.01-1.25)	0.031
AISI mutually adjusted for SILI	1.01 (0.94-1.09)	0.76	1.01 (0.90-1.13)	0.87
SILI mutually adjusted for hs-CRP	1.06 (0.99-1.14)	0.071	1.09 (0.96-1.23)	0.21
hs-CRP mutually adjusted for SILI	1.15 (1.07-1.23)	<0.001	1.10 (0.91-1.33)	0.34

All estimates are from survey-weighted Cox models adjusted as in Model 2 (primary fully adjusted model; age, sex, race/ethnicity, education, poverty-income ratio, BMI, smoking, diabetes, hypertension). Every marker was ln-transformed, standardized within sex against the analytic sample (n=16,479), and entered per 1-SD increment, so that hazard ratios are directly comparable across rows; ferritin and the composite indices enter as continuous standardized exposures. In the mutually adjusted models each comparator (SII, SIRI, AISI, or hs-CRP) was entered together with SILI, for all-cause and cardiovascular mortality; because hs-CRP is itself a component of SILI (survey-weighted r=0.69), the hs-CRP rows decompose a single construct rather than test two independent markers. SILI retained a significant all-cause association after adjustment for each differential-count composite ($P \leq 0.036$), whereas every composite was attenuated to non-significance after adjustment for SILI ($P \geq 0.10$); after adjustment for hs-CRP, SILI was no longer significant (P=0.071) while hs-CRP remained significant ($P < 0.001$), so the hepatic acute-phase axis carries the largest share of the signal. This indicates that the hepatic and iron-metabolic axes carry prognostic information not contained in the differential count.

Mutual adjustment with hs-CRP. Because hs-CRP is itself a component of SILI, the two measures are strongly correlated (survey-weighted r = 0.69), so their mutual adjustment is best read as a decomposition of one construct rather than a test of two independent markers. Entered together in Model 2, hs-CRP kept a significant all-cause association (per 1-SD HR, 1.15; 95% CI, 1.07-1.23; $P < 0.001$) whereas SILI was attenuated (1.06; 0.99-1.14; P = 0.071); for cardiovascular mortality neither estimate was significant (hs-CRP, 1.10; 0.91-1.33; P = 0.34; SILI, 1.09; 0.96-1.23; P = 0.21). Removing the hepatic axis from SILI altogether, the mean of the

ferritin and NLR z-scores remained associated with all-cause mortality (1.07; 1.01-1.13; P = 0.018) and was attenuated to 1.05 (1.00-1.10; P = 0.071) when hs-CRP was added. The hepatic axis therefore carries the largest share of the prognostic information in SILI, but the iron-metabolic and cellular axes are not inert: they remain associated with mortality on their own. SILI should be read as an integrated exposure measure, not as a substitute for hs-CRP.

Incremental predictive performance. Adding SILI to the base covariate model improved continuous NRI at 10 years (0.132; SE, 0.026; P<0.001), driven by upward reclassification of cases (1.6%) and downward reclassification of controls (1.2%; Supplementary Table S3). IDI was small but statistically significant (0.0034; SE, 0.0010; P=0.001). Categorical NRI at the 5% and 10% 10-year risk thresholds was null (0.004; SE, 0.007; P=0.59), which suggests the prognostic gain reflects graded movement within the risk distribution rather than crossing clinically meaningful decision thresholds. SII produced a smaller continuous NRI (0.046; SE, 0.028; P=0.11) and a much smaller IDI (0.0012; P=0.009), so SILI added more incremental prognostic information than the cellular composite alone.

Discrimination over time, calibration, and decision analyses. These analyses quantify how much individual-level prognostic information SILI adds beyond the base model. Time-dependent IPCW AUCs for the base model were 0.892, 0.888, and 0.882 at 5, 10, and 15 years, and 0.893, 0.889, and 0.881 after adding SILI. Differences were 0.001 or less and did not consistently favor the larger model; as with the C-index, the high absolute AUC values largely reflect age. Supplementary Figure S3 extends the comparison to all seven markers: the eight time-dependent AUC curves nearly superimposed over follow-up, and the 10-year AUC ranged only from 0.888 (AISI and SIRI) to 0.890 (hs-CRP), with the base model at 0.888. The 10-year IPCW Brier score was 0.0407 for the base model and 0.0405 for base + SILI. Calibration of the base + SILI model was good across deciles of predicted 10-year risk: predicted risks ranged from 0.22% to 55.1%, and IPCW-observed risks from 0.66% to 57.1%, tracking closely except in the lowest deciles where events were sparse

(Supplementary Figure S1a). Decision-curve analysis showed the base + SILI and base models were essentially superimposed across risk thresholds of 1% to 30% (maximum net benefit difference, 0.0009), and neither offered net benefit over treat-all or treat-none strategies beyond about 6% (Supplementary Figure S1b). Taken together, the positive continuous NRI and IDI indicate that SILI adds statistically detectable prognostic information, but the null categorical NRI, unchanged time-dependent AUC, and identical net benefit mean that this information does not improve individual-level risk discrimination or clinical decision-making in a general population sample.

Threshold effect and absolute risk difference. The two-piecewise Cox model selected a breakpoint at SILI=0.98 (about 1.6 SD above the cohort median of 0.003) for all-cause mortality, with a highly significant improvement over a single-line model (design-based likelihood-ratio test, P<0.001). Below the breakpoint, the hazard ratio per 1-unit increment of SILI (one unit≈1.64 SD) was flat and nonsignificant (1.09; 0.98-1.21); above it, each additional unit was associated with a 6.3-fold hazard (6.27; 4.05-9.72). Cardiovascular mortality selected the same breakpoint, with a flat lower segment (1.08; 0.92-1.27) and a steep upper segment (7.01; 3.28-14.98; P=0.001). These estimates quantify the spline result: the association is not a graded linear effect across the full exposure distribution but is concentrated in the upper tail, where multiple inflammatory pathways may be concurrently activated. In absolute terms, the fully adjusted difference in restricted mean survival time over 12 years was −2.31 months (95% CI, −3.37 to −1.25; P<0.001) for the highest versus lowest SILI quartile, while the continuous parametrization gave −1.01 months per 1-SD increment (95% CI, −1.36 to −0.66; P<0.001). As noted above, these figures come from separate parametrizations of the same pseudo-value regression and are not linearly convertible. The absolute burden is therefore modest at the individual level, consistent with

the negligible discrimination increment and reinforcing that SILI functions as an exposure measure rather than as a risk-prediction tool.

Robustness analyses. When follow-up was split at 5 and 10 years, the association attenuated monotonically with time since baseline: the hazard ratio per 1-SD increment was 1.24 (1.10-1.40; P=0.0005) in the first 5 years, 1.11 (1.00-1.23; P= 0.056) between 5 and 10 years, and 1.10 (1.00-1.22; P=0.049) beyond 10 years. This broad split indicates that the association is concentrated in the first years after baseline and is diluted progressively thereafter, most plausibly by regression dilution. A finer split at 3, 6, and 9 years, which resolves the early decay more sharply, is presented below. Quantitatively, the E-value was 1.51 for the all-cause point estimate and 1.31 for the corresponding confidence limit, and 1.51 and 1.21 for cardiovascular mortality. An unmeasured confounder would therefore need to be associated with both SILI and mortality by a risk ratio of at least 1.51 to explain away the all-cause association entirely, and by 1.31 to shift the confidence interval to include unity.

Additional analyses: dose-response, joint exposure, temporal pattern, landmark, and cause-specific transitions

Quintile and decile dose-response. All-cause hazard ratios increased stepwise across survey-weighted SILI quintiles (Q2 vs Q1: 1.08, 0.88-1.32; Q3: 1.09, 0.93-1.27; Q4: 1.20, 1.02-1.40; Q5: 1.31, 1.11-1.55; P for trend=7.7×10^{-4}). Cardiovascular mortality followed the same pattern (Q4: 1.40, 1.00-1.97, P= 0.049; Q5: 1.36, 1.00-1.86, P=0.052; P for trend= 0.035), while cancer mortality was flat (Q5: 1.11, 0.78-1.57; P for trend =0.83). In decile analyses, all-cause hazard ratios stayed near 1.0 from D2 to D9 (range 0.79-1.10) and rose only in the top decile (D10: 1.29, 0.98-1.69), confirming that the risk gradient is carried by the upper tail rather than by a graded shift across the whole distribution (Figure 4a).

Joint exposure with hs-CRP. When SILI and hs-CRP were cross-classified at their medians, only the double-high group had a significantly increased risk of all-cause death (high

SILI/high CRP: 1.26, 1.09-1.45, P=0.001), compared with high SILI/low CRP (1.10, 0.95-1.28) and low SILI/high CRP (1.12, 0.89-1.40). Elevated hs-CRP thus carried little prognostic information when SILI was low, whereas elevated SILI was weakly informative when hs-CRP was low and clearly informative when both were elevated. The two markers appear to identify overlapping but not identical risk. For cardiovascular mortality, the double-high group was again the only significantly elevated category (1.27, 1.01-1.60, P=0.043). However, there was no departure from additivity: On the additive scale (approximated on the hazard-ratio scale), RERI was 0.04 (−0.26 to 0.34; P=0.79) for all-cause and −0.05 (−0.54 to 0.44; P=0.85) for cardiovascular mortality. The joint pattern is therefore better described as two partly independent markers each contributing to risk rather than as synergy (Figure 4b).

Time-varying association. In a finer time-split analysis at 3, 6, and 9 years, the all-cause hazard ratio per 1-SD increment fell sharply with time since baseline: 2.47 (1.96-3.12) during years 0-3, 1.34 (1.04-1.74) during 3-6, 1.09 (0.93-1.27) during 6-9, and 1.06 (0.99-1.13) beyond 9 years. Cardiovascular mortality showed the same decay (from 2.38 in years 0-3 to 1.01 beyond 9 years). This finer split is complementary to the broader 5/10-year split reported above: the coarse split averages over longer windows and therefore dilutes the strong early effect, whereas the fine split resolves the early peak. Because period-specific estimates cannot be combined with the fully survey-weighted variance estimator, the global SILI×period interaction was formally tested only for the 5/10-year split (P=0.89); the 3/6/9-year split should be read as a descriptive characterization of the temporal gradient rather than as a formal effect-modification test (Figure 4c).

Landmark analyses. Excluding progressively longer early follow-up did not materially change the point estimate: the hazard ratio per 1-SD increment of SILI was 1.135 (1.061-1.213) from baseline, 1.109 (1.037-1.186) after a 12-month landmark (n=16,273; 2,150 deaths), 1.090 (1.021-1.164) after 24 months (n=14,349; 2,034 deaths), and 1.104 (1.024-

1.190) after 60 months (n=11,192; 1,700 deaths); all remained statistically significant. Reverse causation by preclinical disease would be expected to weaken markedly after removing the first years of follow-up; although the persistence of the association across all landmarks attenuated the plausibility of that explanation, residual confounding and complex disease trajectories cannot be fully ruled out, and the overall pattern is more consistent with inflammatory load being related to subsequent mortality risk (Figure 4d).

Cause-specific transitions. Treating vital status as a common origin with two competing destinations, the SILI association was nearly identical across transitions: the hazard ratio per 1-SD increment was 1.132 (1.029-1.246; P=0.011) for cardiovascular death (685 events) and 1.138 (1.060-1.221; P=0.0004) for non-cardiovascular death (1,558 events). The two cause-specific estimates were statistically similar; this pattern does not strongly support a cardiovascular-specific mechanism and is compatible with SILI reflecting broader multi-system vulnerability to death (Figure 4e). This reading is reinforced by the flat cancer-specific quintile trend reported above.

These five analyses leave the central finding unchanged. The dose-response is monotonic but concentrated in the upper tail; SILI and hs-CRP show no additive synergy with each other; the association is strongest early and stable thereafter; it survives landmark exclusion of early deaths; and it is quantitatively the same for cardiovascular and non-cardiovascular death. The complete set of estimates is displayed in Figure 4.

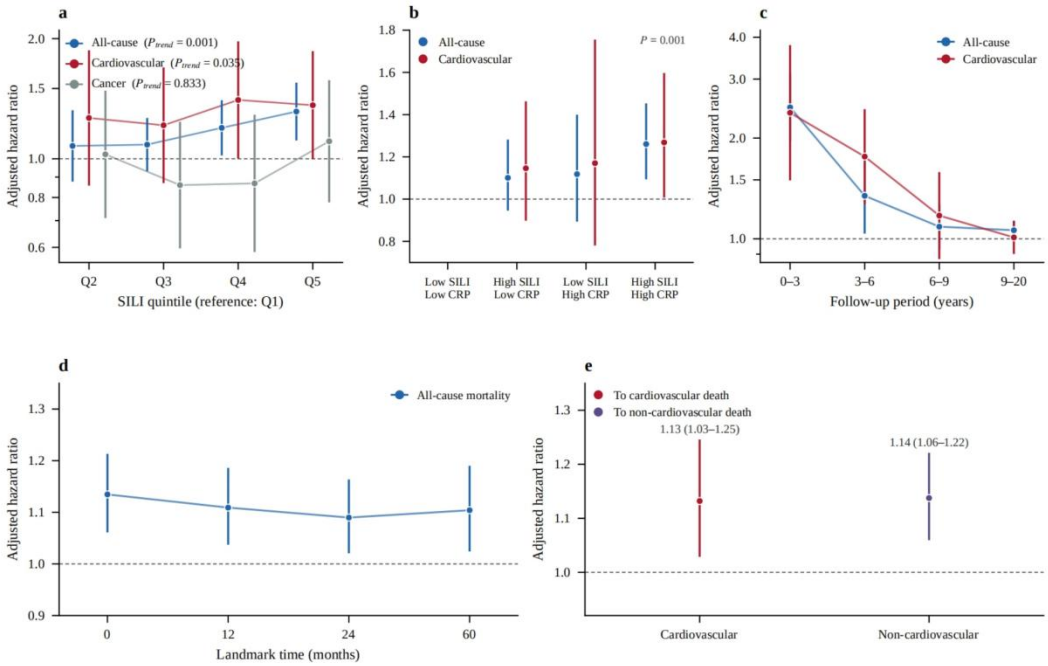


Figure 4. Additional analyses characterizing the SILI-mortality association. (a) Adjusted hazard ratios (HRs) per SILI quintile (reference: Q1) for all-cause, cardiovascular, and cancer mortality (logarithmic y-axis). (b) Joint exposure of SILI and hs-CRP at sex-specific medians; the double-high group shows the only significant risk elevation (all-cause HR 1.26; 95% CI 1.09-1.45) with no additive interaction (RERI 0.04; P=0.79). (c) Period-specific HRs per 1-SD SILI increment after splitting follow-up at 3, 6, and 9 years, demonstrating temporal decay (from 2.47 in years 0-3 to 1.06 in years 9-20). (d) Landmark analyses at 0, 12, 24, and 60 months. (e) Cause-specific transition HRs from the event-free state to cardiovascular versus non-cardiovascular death; estimates are statistically indistinguishable. All models are survey-weighted and adjusted for Model 2 covariates.

Discussion

Principal findings

In this nationally representative cohort of US adults from NHANES 1999-2010 and 2015-2018, we asked whether a simple composite index, the Systemic Inflammatory Load Index (SILI), was associated with mortality. SILI was associated with all-cause and cardiovascular mortality, and the relationship was nonlinear with a threshold-like pattern: risk excess was concentrated above a breakpoint at SILI=0.98, roughly 1.6 SD above the cohort median. Cancer mortality showed no association. In head-to-head comparisons, SILI retained its all-cause association after mutual adjustment for each differential-count composite, while the

competing indices were attenuated to non-significance; reclassification, discrimination, calibration, and decision-analytic metrics are reported below and in the Supplementary Materials. These findings support the use of SILI as a transparent composite measure of multi-system inflammatory burden, with potential value for exposure assessment in etiological research, subject to external validation. We did not set out to replace hs-CRP. hs-CRP remains the strongest single marker in these data, and we propose SILI as an exposure variable that summarises multi-system inflammatory load for etiological research rather than as a risk-prediction instrument.

Comparison with previous studies

To our knowledge, SILI is the first composite to bring together, in a single measure, the hepatic acute-phase response (hs-CRP), the iron-metabolic/reticuloendothelial response (ferritin), and innate-adaptive cellular activation (NLR), and to benchmark it head-to-head against existing composites within one nationally representative cohort. The existing composites, SII, SIRI, and AISI, rely solely on the complete blood count and capture only the cellular arm of inflammation. Three related indices differ from SILI in definable ways. The Inflammatory Burden Index (IBI) combines CRP with neutrophil and lymphocyte counts, covering the hepatic and cellular axes but not iron metabolism [28]; the C-reactive protein-albumin-lymphocyte (CALLY) index combines CRP, albumin, and lymphocytes, adding a nutritional axis but again omitting iron metabolism [29]; and the Pan-Immune-Inflammation Value (PIV) combines neutrophil, platelet, and monocyte counts and therefore covers only the cellular arm [30]. None of the three spans all three axes at once, and none has been compared with a multi-axis composite within a single cohort. In the head-to-head mutual-adjustment models, the pattern was asymmetric: SILI kept its all-cause association after adjustment for each differential-count composite, whereas those composites were attenuated to non-significance after adjustment for SILI. This suggests SILI may capture inflammatory

information beyond the cellular component, not that the cellular axis is biologically contained within SILI. Joint-exposure analysis showed that only participants high on both SILI and hs-CRP were at significantly elevated risk, with no additive interaction; for the mortality endpoint the hepatic acute-phase axis therefore carries the dominant share of the signal, as the mutual-adjustment models make explicit. The dose-response pattern was monotonic but carried almost entirely by the top decile, and spline and two-piecewise analyses converged on a threshold above the cohort median. This threshold-like pattern fits a scenario in which compensatory regulatory processes may dampen risk at lower inflammatory burdens, while concurrent activation across the hepatic, iron-metabolic, and cellular pathways may signal a systemic inflammatory state associated with vascular injury. A single marker such as hs-CRP, which captures only one pathway, would be expected to show a more graded, linear association. In the exposure-measurement sense, SILI summarizes three partly independent pathways and cannot be replaced by any single marker or by a purely cellular composite, even though, for mortality, the hepatic axis contributes most of the prognostic signal. Consistent with the prespecified equal-weighting design, SILI was conceived as an exposure measure rather than a statistically optimized predictor; detailed reclassification, discrimination, calibration, and decision-analytic comparisons are provided in the Results and Supplementary Materials.

Beyond these construct-level comparisons, our findings extend the single-marker evidence: elevated hs-CRP predicts total and cardiovascular death [5], elevated NLR carries prognostic information in acute and chronic disease [31-33], and ferritin showed a null single-component association after full adjustment, consistent with its U-shaped relation with cardiometabolic risk. The prespecified SILI-2 variant produced slightly stronger estimates, but ferritin was retained in the primary index to preserve construct completeness, with SILI-2 positioned as a prediction-oriented alternative.

Biological plausibility

Biologically, the three components sit at complementary nodes of the systemic inflammatory network, chosen because they are the best-characterized and most widely measured dimensions of systemic inflammation. IL-6-driven hepatocyte CRP secretion marks chronic cytokine activation [34,35]; ferritin synthesis is co-regulated by pro-inflammatory cytokines and iron status, linking inflammation to iron sequestration and hepcidin biology [36]; and neutrophil expansion with relative lymphopenia reflects stress hematopoiesis and impaired adaptive immunity, processes implicated in atherogenesis and plaque instability [37,38]. A composite of these axes may approximate inflammatory load more faithfully than any single marker, which may explain the threshold-like pattern. The downstream effector domains and upstream drivers are summarized in Supplementary Figure S6; mechanistic pathways plausibly supported by the present data (weak inter-axis correlations, upper-tail risk excess, and comparable associations with cardiovascular and non-cardiovascular mortality) are rendered as thick solid lines, while remaining pathways represent speculative or literature-derived links and are shown as thin solid lines.

Strengths and limitations

This study has several strengths: nationally representative sampling with complex-survey weighting, long follow-up with NDI-adjudicated mortality, a simple and reproducible index based on routine assays, a prespecified analysis plan with equal weighting and defined cutoffs, comprehensive sensitivity analyses, and head-to-head benchmarking of seven inflammatory markers with mutual adjustment and absolute risk differences. These strengths should be weighed against several limitations. The observational design precludes causal inference. The mortality association was largely carried by the hs-CRP component, and in mutual adjustment SILI did not retain significance once hs-CRP was taken into account, so SILI should not be read as a substitute for that marker. Exposures were measured once at baseline, so regression dilution may attenuate estimates; hypertension was self-reported. The

2011-2014 cycles were unavailable, the 2015-2018 stratum had limited precision, and ferritin assay restrictions produced a predominantly female sample, limiting generalizability. Some subgroup and cancer analyses were underpowered; the data-driven breakpoint was not internally validated and should be regarded as a descriptive characterization rather than a validated cut-point; equal weighting favors simplicity; and reclassification and discrimination metrics did not show meaningful individual-level improvement. SILI is therefore positioned for etiological and exposure-oriented research rather than individual-level risk prediction.

This nationally representative cohort study found that higher composite systemic inflammatory load, quantified by SILI, was associated with all-cause and cardiovascular mortality in a threshold-like manner. The mutually adjusted models suggest SILI may capture inflammatory information beyond the cellular component, and the joint-exposure analysis indicates that, for the mortality endpoint, the signal is carried mainly by the hepatic acute-phase axis, so SILI is not a substitute for hs-CRP. Together with its biological plausibility, these findings support interpreting SILI as a composite reflecting multi-system inflammatory burden, with potential use in exposure assessment for etiological research, subject to external validation.

What SILI adds, and for whom. SILI does not add predictive power: Delta C was approximately zero and the time-dependent AUC was unchanged. Its value is as a single, transparent exposure variable for population-based etiological research, in three ways. First, cohort studies that already measure hs-CRP, ferritin, and a differential count can replace three correlated exposures with one pre-specified variable, avoiding selective reporting of whichever single marker reaches significance. Second, because SILI spans three axes, it can serve as the exposure in studies of upstream social, metabolic, or environmental determinants, where a single marker would capture only one pathway. Third, it can be used as an effect modifier or intermediate exposure in analyses of inflammatory mechanisms, as the mutual-adjustment and joint-exposure results illustrate. SILI requires only routine assays and is computed from cohort-internal sex-specific z-scores, so it is reproducible in any cohort that measures the three components; it should not be used for individual-level risk prediction.

Methods

Study design and population

We selected NHANES 1999-2010 and 2015-2018 because these are the only cycles with both hs-CRP and ferritin publicly available; the 2011-2014 cycles were excluded due to the

absence of ferritin assay files, as NHANES neither measured nor released serum ferritin and listed no hs-CRP assay file in the per-cycle public-use laboratory documentation [17]. Mortality status was ascertained by probabilistic linkage to the National Death Index through December 31, 2019 [18]. Individuals who did not attend the MEC examination (n=3,770), were younger than 20 years or pregnant at examination (n=37,471), were ineligible for mortality linkage (n=89), had missing hs-CRP, ferritin, or a valid differential cell count or had hs-CRP>10 mg/L (n=21,420), or had missing any model covariate (n=2,156) were excluded from the analysis. The NHANES protocol was approved by the Research Ethics Review Board of the US Centers for Disease Control and Prevention's National Center for Health Statistics. Written informed consent was obtained from all adult participants. This study followed the Strengthening the Reporting of Observational Studies in Epidemiology (STROBE) reporting guideline for cohort studies.Finally, a total of 16,479 adults were included in the study (Figure 1).

A structural feature of the source data shapes the sex composition of the cohort. Serum ferritin was assayed in all examined adults in 1999-2002 [19] and 2017-2018 [20], but in the five intermediate cycles (2003-2004, 2005-2006, 2007-2008, 2009-2010, and 2015-2016) the assay was restricted to children and women of childbearing age (12-49 years) [19,21]. Adult men and women aged≥50 years in those cycles therefore had no ferritin measurement and could not contribute to the three-component index. As a result, the analytic sample comprised 66.4% women (unweighted; 67.2% weighted), with male participants drawn only from the 1999-2002 and 2017-2018 cycles. A prespecified sensitivity analysis restricted to the three ferritin-complete cycles assessed the influence of this sex composition (Methods, Statistical analysis; Results, Sensitivity analyses and single components).

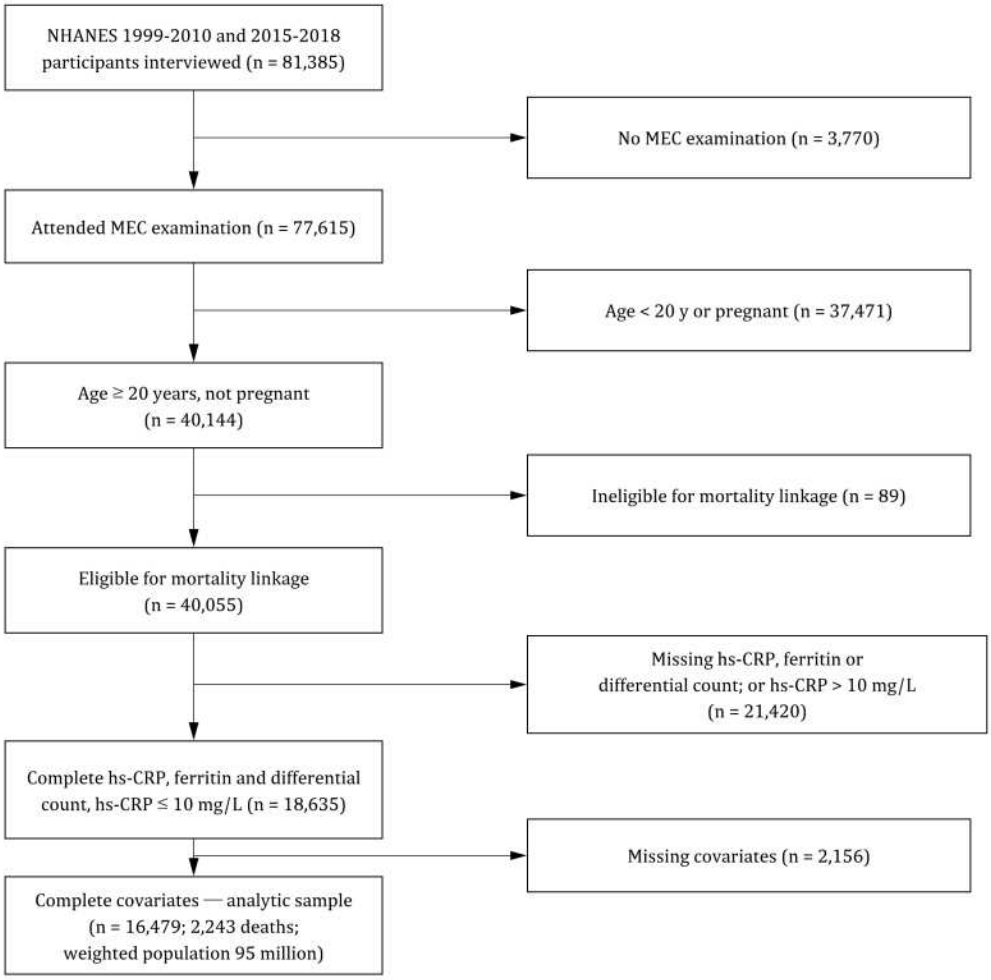


Figure 1. The analytic cohort comprised 16,479 US adults (weighted population 95 million) followed for up to 20 years (median 12.1 years; 2,243 deaths). The flow chart shows how this sample was reached: NHANES 1999-2010 and 2015-2018 participants were sequentially restricted to MEC-examined adults aged ≥ 20 years eligible for mortality linkage with complete hs-CRP, ferritin, and differential counts (hs-CRP ≤ 10 mg/L) and complete covariates.

Exposure: the Systemic Inflammatory Load Index

SILI was built from three widely measured inflammatory markers: serum hs-CRP (mg/L), reflecting the hepatic acute-phase response; serum ferritin (ng/mL), reflecting iron storage and the reticuloendothelial acute-phase response; and the NLR from the automated complete blood count, reflecting innate-adaptive immune activation. All three markers were ln-transformed to reduce right skew and then standardized within sex using means and standard deviations derived from the present analytic sample (n=16,479), rather than an external

reference population. This places the three components on a common, fully reproducible scale. SILI was calculated as the arithmetic mean of the three z-scores. Because the z-scores are defined relative to this cohort, SILI is a cohort-internal relative measure; raw values are not directly comparable across cohorts. The between-person SD of SILI was 0.61. Effect estimates are reported per 1-SD increment and by weighted quartiles (cut-points: −0.407, 0.003, 0.400).

Equal weighting of the three components was a prespecified design choice. SILI was conceived as an exposure measure that summarizes the overall multi-system inflammatory load, not as a statistically optimized predictor. We therefore did not derive weights from outcome data, which avoids overfitting and prevents circularity from weighting a biomarker by its association with the outcome under study; the index stays transparent and reproducible. Ferritin was retained with equal weight on a priori grounds. It is an acute-phase protein co-regulated with CRP by interleukin-6 and the principal readout of the iron-inflammation axis (hepcidin biology). As the weak correlations among the three z-scored components show (Results), ferritin carries metabolic information orthogonal to the hepatic and cellular arms, even though its single-marker association with mortality is null in fully adjusted models. Because equal weighting can let a null component dilute the composite, we prespecified a two-component variant excluding ferritin (SILI-2, the mean of the hs-CRP and NLR z-scores) and report it alongside SILI in sensitivity analyses. To avoid ambiguity: the three-component SILI is the primary exposure; SILI-2 is a prespecified sensitivity variant used only to quantify the effect of including ferritin.

Outcomes

The primary outcome was all-cause mortality. Secondary outcomes were cardiovascular mortality (underlying cause-of-death codes 001-005 of the NDI underlying cause of death recode: diseases of heart and cerebrovascular diseases) and cancer mortality (code 002,

malignant neoplasms). Person-time accrued from the MEC examination date to death or December 31, 2019; participants with zero months of follow-up were assigned 0.5 months.

Covariates

Covariates were selected a priori as confounders or precision variables for the association between SILI and mortality. Continuous variables included age (years), body mass index (BMI, kg/m²), and family poverty-income ratio (capped at 5). Categorical variables included sex (male, female), race/ethnicity (non-Hispanic White, non-Hispanic Black, Mexican American, other Hispanic, other), education (<9th grade, 9-12th grade, high school, some college, ≥college), and smoking status (never, former, current). Diabetes was defined as a self-reported diagnosis or HbA1c≥6.5%. Hypertension was defined by self-report of a prior physician diagnosis only. Measured blood pressure values were not included in the primary covariate set; this limitation and its likely direction of bias are detailed in Discussion, Strengths and limitations. Baseline prevalent cardiovascular disease (self-reported coronary heart disease, heart attack, heart failure, or stroke) and cancer were used for sensitivity analyses.

Statistical analysis

Data were analyzed using R software (version 4.3.3) with the "survey" package, following NHANES analytic guidelines. Because NHANES used a complex, multistage probability sampling design to select representative participants, we incorporated primary sampling units, strata, and sample weights. Because eight cycles were pooled, MEC examination weights were divided by eight (WTMEC2YR/8), as recommended for combining multiple survey cycles. Variance strata were defined as survey cycle crossed with the native stratum variable (SDMVSTRA), and masked variance units (SDMVPSU) served as clusters, with the finite-population correction approximated by the with-replacement design and the "lonely PSU" adjustment. Weighted analyses used the survey package to generate nationally representative

estimates. Differences in categorical variables were assessed with the chi-square test; differences in continuous variables with one-way ANOVA for normally distributed variables and the Kruskal-Wallis test for non-normally distributed variables.

Survey-weighted Cox proportional hazards models were used to estimate hazard ratios (HRs) and 95% confidence intervals (CIs). SILI entered the models in two ways: per 1-SD increment and as weighted quartiles, with a test for linear trend across quartile ordinal. Model 1 included age, sex, and race/ethnicity. Model 2 added education, poverty-income ratio, BMI, smoking status, diabetes, and hypertension; this was the primary fully adjusted model. Model 3 added baseline prevalent cardiovascular disease and cancer. The crude model and Models 1-3 are all reported in Table 2. Because age, BMI, diabetes, and hypertension were prespecified as confounders rather than mediators, we did not run formal mediation analyses. For non-linearity, we used restricted cubic splines with internal knots at the 25th, 50th, and 75th percentiles and boundary knots at the observed minimum and maximum, compared with linear models using likelihood-ratio survey Wald/LRT tests; HRs were referenced to the cohort median. Inverse-probability-weighted Kaplan-Meier curves compared survival across SILI quartiles and were used for visualization only; all statistical inference came from the Cox models. Subgroup analyses tested SILI×subgroup interactions for age (<60 vs ≥60 years), sex, race/ethnicity, diabetes, obesity (BMI <30 vs ≥30 kg/m²), and smoking. Race/ethnicity was collapsed to three groups (non-Hispanic White, non-Hispanic Black, and all other groups combined) for interaction tests only; smoking kept three levels (never, former, current). These two three-level variables each produced two interaction terms, yielding eight tests, all subgroup interaction P values were corrected for multiple comparisons using the Benjamini-Hochberg false discovery rate procedure. All cutoffs (age 60 years, BMI 30 kg/m², hs-CRP 10 and 3 mg/L, and the 24-month landmark) were prespecified before analysis. Two-sided $P<0.05$ defined statistical significance.

We ran several prespecified sensitivity analyses. First, to limit reverse causation, we censored all events before 24 months rather than excluding participants. Second, we restricted the sample to hs-CRP≤3mg/L. Third, we excluded participants with prevalent cardiovascular disease, cancer, or both. Fourth, we applied multiple imputation by chained equations to the pre-MI sample (n=18,635). Age, sex, race/ethnicity, and hypertension were complete; missingness was limited to education (n=33), poverty-income ratio (n =1,760), BMI (n=386), smoking (n=19), and diabetes (n=23). The imputation model included Model 2 covariates plus age, sex, race/ethnicity, SILI, mortality status, and follow-up time. Estimates were combined using Rubin's rules. We used m=5 and a confirmatory m=20; results were virtually identical. Fifth, we modeled cardiovascular mortality with Fine-Gray subdistribution hazards, treating non-cardiovascular deaths as competing events and multiplying survey weights by the inverse probability of censoring weights. This yields subdistribution hazard ratios, which estimate the effect on cumulative incidence of cardiovascular death rather than the instantaneous hazard. We also estimated survey-weighted Aalen-Johansen cumulative incidence functions by SILI quartile (Supplementary Figure S2). Sixth, we fitted single-component models for hs-CRP, ferritin, and NLR, and calculated Harrell C-indices for the base model with and without SILI, and for hs-CRP alone. Seventh, we fitted SILI-2 (hs-CRP and NLR) to assess ferritin's influence. Eighth, we repeated the main all-cause analysis separately in 1999-2010 and 2015-2018 to check for drift. Ninth, we restricted to the three cycles with ferritin measured in both sexes (1999-2002, 2017-2018) to assess the influence of female over-representation. In addition, we fitted the seven-marker benchmark (Table 3), and the reclassification, calibration, time-dependent discrimination, decision-curve, threshold, restricted-mean-survival, time-split, negative-control, and alternative-standardization analyses described above, and computed E-values. We also report survey-weighted Pearson correlations among the three z-scored components, overall and by sex. Two-sided $P < 0.05$

defined significance. Analyses used R 4.3.3 (survey, survival, mice) and Python 3.11 for figures. Tenth, because hypertension was defined by self-report in the primary models, we additionally adjusted for measured systolic and diastolic blood pressure (MEC examination) and for current use of antihypertensive medication (BPQ040A), variables that were not part of the primary covariate set.

Benchmarking against alternative inflammatory indices. To place SILI alongside existing composites, we constructed three differential-count indices as originally proposed: SII , SIRI, and AISI. Each was ln-transformed, standardized within sex, and entered per 1-SD increment, so all seven markers (SILI, hs-CRP, ferritin, NLR, SII, SIRI, AISI) were scaled identically and compared under the same Model 2 covariate set for all-cause, cardiovascular, and cancer mortality. Because these composites are highly correlated by construction, we also fitted mutually adjusted models containing SILI with each competing index in turn, isolating SILI's contribution beyond the cellular axis. Discrimination was compared using Harrell C-indices for each base + single-marker model; we report increments (ΔC) rather than absolute values because the base model already includes strong predictors such as age.

Incremental predictive performance, calibration, and decision analysis. Among participants with determinate 10-year mortality status, we computed continuous and categorical NRI and IDI for base + SILI versus the base covariate model, and for base + SII versus the base model for comparison, using design-based estimators (survey-weighted means or differences of means) [22,23]. Model-specific baseline cumulative hazards were used to convert linear predictors into 10-year absolute risks, placing the compared models on a common risk scale; the categorical NRI used 5% and 10% 10-year risk thresholds. Time-dependent discrimination was quantified using IPCW-based AUCs at 5, 10, and 15 years, with IPCW weights derived from the Kaplan-Meier estimator of the censoring distribution [24]; this metric was computed for the base model and for each base + single-marker model

across all seven markers (SILI, hs-CRP, ferritin, NLR, SII, SIRI, and AISI; Supplementary Figure S3). Calibration was assessed by comparing mean predicted with IPCW-observed 10-year risk across deciles, and overall accuracy by the IPCW Brier score [25,26]. Decision-curve analysis computed net benefit across 10-year risk thresholds of 1-30%, with the denominator set to the total survey weight so that net benefit is computed on the weighted population scale [27]. Because this is a general population sample, these metrics characterize prognostic information content rather than clinical utility.

We formalized the threshold pattern suggested by the spline using a two-piecewise linear Cox model. Candidate breakpoints were searched across the 5th-95th percentiles of SILI; at each breakpoint k, exposure was represented by min(SILI, k) and max(SILI-k, 0). The breakpoint minimizing survey-design deviance was selected, and improvement over a single-line model was tested with a design-based likelihood-ratio test. As a negative control, we used accidental death (NDI recode category 4); a null association would argue against a generic unmeasured-confounding artefact. To express the association in absolute terms, we estimated the difference in restricted mean survival time over 12 years (τ=144 months) using jackknife pseudo-values from leave-one-out Kaplan-Meier estimation, regressed on SILI with survey design and Model 2 covariates. We repeated the primary estimate within 0-5, 5-10, and ≥10-year follow-up periods, compared period-specific hazard ratios, and tested the global SILI×period interaction; a two-piecewise reconstruction was used because interaction terms cannot be estimated with the fully survey-weighted variance estimator under left truncation. To check whether sex-stratified z-standardization generated the findings, we rebuilt SILI using overall standardization (r=0.96 with primary SILI) and repeated the main models. Finally, we computed E-values for the all-cause and cardiovascular point estimates and lower confidence limits.In addition, we performed a second time-split analysis using 3-, 6-, and 9-year cutoffs, yielding period-specific hazard ratios for 0-3, 3-6, 6-9, and 9-20 years. The

5/10-year split provides broad period estimates, whereas the 3/6/9-year split is finer and is intended to characterize the early decay of the association. The two splits are complementary: the coarse split averages over longer windows, whereas the fine split resolves the early peak. Because period-specific estimates cannot be combined with the fully survey-weighted variance estimator under left truncation, the global SILI×period interaction was formally tested only for the 5/10-year split; the 3/6/9-year split is descriptive.

Dose-response, joint-exposure, temporal, landmark, and transition analyses. We modeled SILI in survey-weighted quintiles (and deciles for all-cause mortality) with the lowest category as reference; trend tests used the median SILI of each category as a continuous term. Since hs-CRP is the most available component, we cross-classified participants at sex-specific cohort medians of SILI and hs-CRP into four groups (low/low, high SILI/low CRP, low SILI/high CRP, high/high) and fitted one Cox model with this four-level joint-exposure term. Additivity departure was quantified as RERI=HR(high/high) − HR(high/low)−HR(low/high) +1, with delta-method variance and a two-sided P value. RERI was approximated on the hazard-ratio scale under the rare-outcome assumption.For time-varying association, we split follow-up at 3, 6, and 9 years (survSplit) and fitted period-specific SILI terms, giving hazard ratios for 0-3, 3-6, 6-9, and 9-20 years. Landmark analyses (a supporting analysis) repeated the main model among participants alive and event-free at 0, 12, 24, and 60 months, removing early deaths and isolating the association from reverse causation by preclinical disease. NHANES records only vital status and a single underlying cause of death and does not observe intermediate non-fatal cardiovascular events, so a full illness-death multistate model is not identifiable. We therefore did not fit a multistate model. Instead, we fitted a simplified three-state structure (alive and event-free → cardiovascular death; alive and event-free → non-cardiovascular death) as cause-specific transition hazards from a common origin state. This structure estimates cause-specific hazards rather than

transition probabilities of a full multistate process, and it was used only to compare the SILI association across the two competing transitions within the cohort.

Data availability

The datasets analysed during the current study are publicly available from the National Center for Health Statistics: NHANES survey data (https://wwwn.cdc.gov/nchs/nhanes/) and the public-use linked mortality files (https://www.cdc.gov/nchs/data-linkage/mortality-public.htm). Analysis code is available from the corresponding author on reasonable request.

References

1. Ajoolabady A, Pratico D, Tang D, Zhou S, Franceschi C, Ren J. Immunosenescence and inflammaging: Mechanisms and role in diseases. Ageing Res Rev. 2024;101:102540. doi:10.1016/j.arr.2024.102540
2. Ferrucci L, Fabbri E. Inflammageing: chronic inflammation in ageing, cardiovascular disease, and frailty. Nat Rev Cardiol. 2018;15(9):505-522.
3. Singh A, Schurman SH, Bektas A, et al. Aging and Inflammation. Cold Spring Harb Perspect Med. 2024;14(6):a041197. doi:10.1101/cshperspect.a041197
4. Ridker PM, Bhatt DL, Pradhan AD, et al. Inflammation and cholesterol as predictors of cardiovascular events among patients receiving statin therapy: a collaborative analysis of three randomised trials. Lancet. 2023;401(10384):1293-1301. doi:10.1016/S0140-6736(23)00215-5.
5. Kurt B, Reugels M, Schneider KM, et al. C-reactive protein and cardiovascular risk in the general population. Eur Heart J. 2025 ;47(15):1799-1810. doi: 10.1093/eurheartj/ehaf937.
6. Qin P, Ho FK, Celis-Morales CA, Pell JP. Association between systemic inflammation biomarkers and incident cardiovascular disease in 423,701 individuals: evidence from the UK biobank cohort. Cardiovasc Diabetol. 2025;24(1):162. doi:10.1186/s12933-025-02721-9
7. Nøst TH, Alcala K, Urbarova I, et al. Systemic inflammation markers and cancer incidence in the UK Biobank. Eur J Epidemiol. 2021;36(8):841-848. doi:10.1007/s10654-021-00752-6.
8. Wu YL, Xiao L, Li HN, Chen LX. Implications of ferritinophagy in cardiovascular diseases and its pharmacological modulation: underlying mechanisms and clinical translation strategies. Cell Mol Biol Lett. 2026;31(1):102. doi:10.1186/s11658-026-00941-9.
9. Suárez-Ortegón MF, McLachlan S, Fernandez-Real JM, Tuomainen TP, Aregbesola A, Wild SH. Serum ferritin and incident cardiometabolic diseases in Scottish adults. Cardiovasc Diabetol. 2022;21(1):26. doi:10.1186/s12933-022-01450-7
10. Cheng ETW, Au CT, Chan RNC, et al. Ferritin is a potential marker of cardiometabolic risk in adolescents and young adults with sleep-disordered breathing. Sleep Adv. 2024;5(1):zpae048. doi:10.1093/sleepadvances/zpae048.
11. Ridker PM, Rane M. Interleukin-6 Signaling and Anti-Interleukin-6 Therapeutics in Cardiovascular Disease. Circ Res. 2021;128(11):1728-1746. doi:10.1161/CIRCRESAHA.121.319077
12. Balla J, Jeney V, Varga Z, Komódi E, Nagy E, Balla G. Iron homeostasis in chronic inflammation. Acta Physiol Hung. 2007;94(1-2):95-106. doi:10.1556/APhysiol.94.2007.1-2.9
13. Hwang M, Canzoniero JV, Rosner S, et al. Peripheral blood immune cell dynamics reflect antitumor immune responses and predict clinical response to immunotherapy. J Immunother Cancer. 2022;10(6):e004688. doi:10.1136/jitc-2022-004688.
14. Ramezankhani A, Tohidi M, Hadaegh F. Association between the systemic immune-inflammation index and metabolic syndrome and its components: results from the multi-ethnic study of atherosclerosis (MESA). Cardiovasc Diabetol. 2025;24(1):78. doi:10.1186/s12933-025-02629-4.
15. Xie Y, Zhang J, Jia J, et al. Combined triglyceride-glucose index and systemic inflammation response index are associated with coronary artery stenosis severity in acute coronary syndrome: a retrospective cohort study. Eur J Med Res. 2025;31(1):88. doi:10.1186/s40001-025-03650-9.

16. Su Z, Cao L, Chen H, et al. Obesity indicators mediate the association between the aggregate index of systemic inflammation (AISI) and type 2 diabetes mellitus (T2DM). Lipids Health Dis. 2025;24(1):176. doi:10.1186/s12944-025-02589-4.
17. Mei Z, Addo OY, Jefferds ME, Sharma AJ, Flores-Ayala RC, Brittenham GM. Physiologically based serum ferritin thresholds for iron deficiency in children and non-pregnant women: a US National Health and Nutrition Examination Surveys (NHANES) serial cross-sectional study. Lancet Haematol. 2021;8(8):e572-e582. doi:10.1016/S2352-3026(21)00168-X.
18. National Center for Health Statistics. Public-use linked mortality file. Hyattsville, MD: US Department of Health and Human Services, CDC; 2019. https://www.cdc.gov/nchs/data-linkage/mortality-public.htm.
19. Centers for Disease Control and Prevention. Second National Report on Biochemical Indicators of Diet and Nutrition in the U.S. Population: Trace Elements in Blood and Serum. Atlanta, GA: US Department of Health and Human Services, CDC; 2012.
20. National Center for Health Statistics. Ferritin & Transferrin Receptor Data (2017-2018): FERTIN_J documentation. Hyattsville, MD: NCHS; 2020. https://wwwn.cdc.gov/Nchs/Nhanes/2017-2018/FERTIN_J.htm.
21. National Center for Health Statistics. Ferritin & Transferrin Receptor Data (2015-2016): FERTIN_I documentation. Hyattsville, MD: NCHS; 2017. https://wwwn.cdc.gov/Nchs/Nhanes/2015-2016/FERTIN_I.htm.
22. Pencina MJ, D'Agostino RB Sr, D'Agostino RB Jr, Vasan RS. Evaluating the added predictive ability of a new marker: from area under the ROC curve to reclassification and beyond. Stat Med. 2008;27(2):157-212. doi:10.1002/sim.2929.
23. Pencina MJ, D'Agostino RB Sr, Steyerberg EW. Extensions of net reclassification improvement calculations to measure usefulness of new biomarkers. Stat Med. 2011;30(1):11-21. doi:10.1002/sim.4085.
24. Yang Z, Rizopoulos D, Newcomb LF, Erler NS. Time-Dependent Predictive Accuracy Metrics in the Context of Interval Censoring and Competing Risks. Biom J. 2026;68(1):e70108. doi:10.1002/bimj.70108.
25. Prince T, Bommert A, Rahnenführer J, Schmid M. On the estimation of inverse-probability-of-censoring weights for the evaluation of survival prediction error. PLoS One. 2025;20(1):e0318349. doi:10.1371/journal.pone.0318349.
26. Pate A, Sperrin M, Riley RD, et al. Calibration plots for multistate risk predictions models. Stat Med. 2024;43(14):2830-2852. doi:10.1002/sim.10094.
27. Vickers AJ, Van Claster B, Wynants L, Steyerberg EW. Decision curve analysis: confidence intervals and hypothesis testing for net benefit. Diagn Progn Res. 2023;7(1):11. doi:10.1186/s41512-023-00148-y.
28. Li W, Zhao D, Li W. Inflammatory burden index predicts long term mortality in a nationally representative population from NHANES. Sci Rep. 2025;15(1):25034. doi:10.1038/s41598-025-09574-y.
29. Huang D, Wu H, Zhou J, Yin S, Wang R, Quan Z. Negative association of C-reactive protein-albumin-lymphocyte index (CALLY index) with all-cause and cardiovascular mortality in population with CKD: the mediating role of biological age acceleration. Ren Fail. 2025;47(1):2586892. doi:10.1080/0886022X.2025.2586892.
30. Dai J, Sun X, Lin B, Sun Y, Chen L. Pan-immune-inflammation value is associated with all-cause and cause-specific mortality among individuals with cancer survivors: a population-based longitudinal cohort study. Cancer Treat Res Commun. 2026;46:101070. doi:10.1016/j.ctarc.2025.101070

31. Firment J, Hulin I. Zahorec index or Neutrophil-to-lymphocyte ratio, valid biomarker of inflammation and immune response to infection, cancer and surgery. Bratisl Lek Listy. 2024;125(2):75-83. doi:10.4149/BLL_2024_012
32. Hoesterey DT, Dang H, Markovic D, et al. Neutrophil-to-Lymphocyte Ratio as a Biomarker in Clinically Stable Chronic Obstructive Pulmonary Disease: SPIROMICS Cohort. Ann Am Thorac Soc. 2025;22(12):1881-1890. doi:10.1513/AnnalsATS.202412-1265OC.
33. Gosav EM, Tanase DM, Buliga-Finis ON, et al. The Prognostic Role of the Neutrophil-to-Lymphocytes Ratio in the Most Frequent Cardiovascular Diseases: An Update. Life (Basel). 2024;14(8):985. doi:10.3390/life14080985.
34. Ngwa DN, Pathak A, Agrawal A. IL-6 regulates induction of C-reactive protein gene expression by activating STAT3 isoforms. Mol Immunol. 2022;146:50-56. doi:10.1016/j.molimm.2022.04.003
35. Wensveen FM, Šestan M, Polić B. The immunology of sickness metabolism. Cell Mol Immunol. 2024;21(9):1051-1065. doi:10.1038/s41423-024-01192-4
36. Hortová-Kohoutková M, Skotáková M, Onyango IG, et al. Hepcidin and ferritin levels as markers of immune cell activation during septic shock, severe COVID-19 and sterile inflammation. Front Immunol. 2023;14:1110540. doi:10.3389/fimmu.2023.1110540
37. Gerhardt T, Haghikia A, Stapmanns P, Leistner DM. Immune Mechanisms of Plaque Instability. Front Cardiovasc Med. 2022;8:797046. Published 2022 Jan 11. doi:10.3389/fcvm.2021.797046.
38. Cao H, Meng X, Ma Y, et al. Neutrophil elastase-activatable ratiometric photoacoustic nanoprobes for imaging atherosclerotic plaque vulnerability. Nat Commun. 2025;16(1):9635. doi:10.1038/s41467-025-64633-2.

Author contributions

J.Y. and Y.K. conceived the study. Q.P. and Y.K. designed the analysis. Y.K. performed the statistical analysis and wrote the first draft. J.Y. and Q.P. critically revised the manuscript. All authors read and approved the final manuscript.

Funding

This research received no specific grant from any funding agency in the public, commercial, or not-for-profit sectors.

Acknowledgements

We thank the NHANES participants and the staff of the National Center for Health Statistics.

Competing interests

The authors declare that they have no competing interests.

Ethics approval and consent to participate

The study protocol was approved by the NHANES Institutional Review Board, and was performed in accordance with the Declaration of Helsinki, with all NHANES participants providing signed informed consent.

Supplementary Files

This is a list of supplementary files associated with this preprint. Click to download.

- Supplementarymaterial.docx